Far-infrared properties of lattice resonant modes. VI. Hydrostatic pressure effects*

A. M. Kahan,† M. Patterson,‡ and A. J. Sievers
Laboratory of Atomic and Solid State Physics and Materials Science Center, Cornell University, Ithaca, New York 14853
(Received 17 June 1976)

The frequency shifts produced by hydrostatic pressure have been measured for four resonant-mode systems NaCl:Cu^+, KBr:Li^+, KI:Ag^+, and CsI:Tl^+. The experimental results have been successfully characterized with an anharmonic-oscillator model. Shifts have also been measured for the tunneling and excited-state modes of KCl:Li^+. The tunneling mode [1.15 cm^{-1} for $(^6Li)^+$ at zero strain] increases to 30 cm^{-1} at 1.1% strain. An extra low-frequency transition provides direct evidence that the tunneling levels in the lowest manifold are not equally spaced. We find that the double-harmonic-oscillator model which has been used previously to describe the tunneling levels does not adequately describe the pressure dependence of the five observed absorption lines in KCl:Li^+. Analysis of the data indicates that the off-center Li^+ ion goes on-center with application of a 0.5% strain. At 0.65% strain the KCl:Li^+ spectrum is virtually identical to the KBr:Li^+ spectrum at zero strain.

I. INTRODUCTION

In this paper, we report on the influence of hydrostatic pressure on low-lying monatomic defect modes in alkali halide crystals. Previous investigations have focused on either the on-center type of motion where the impurity ion replaces a host-lattice ion at the vacated lattice position or the off-center or tunneling type of defect where the impurity lies away from the normal lattice site in one of several equivalent positions.[1] Our investigation bridges the gap between the two types of impurity motion by employing hydrostatic pressure to make relatively large changes in the interionic lattice constant and consequently in the local impurity potential of both types of defects. The effects of these changes are monitored by means of the far-infrared absorption spectra associated with impurity motion.

Three methods of changing the local lattice constant around an impurity are uniaxial stress, crystal alloying, and hydrostatic pressure. Uniaxial stress allows the most complete determination of the local symmetry but the range of stress is severely limited by crystal strength to roughly 0.1% change in lattice parameter. This change is too small to appreciably alter the local potential.[2] The substitution of an alkali halide of a different lattice parameter from the host crystal results in a change in lattice parameter in the direction of the substituted crystal's lattice parameter according to Vegard's law. Large changes have been produced with this technique but unfortunately the strains introduced are not uniform. Random components occur which greatly broaden the spectral features in the far infrared and make alloying of limited value.[3] Hydrostatic pressure avoids the difficulties of alloying while providing the largest uniform strains ~1.2%. The main problem with hydrostatic measurements is experimental; it is difficult to work with high-pressure optical cells at low temperatures in the far infrared. This is the first complete report of such a venture with defect modes.

In 1965, low-lying ionic states were discovered in KCl:Li^+,[4,5] and KBr:Li^+,[6] and there has been a long history of experiments and theoretical calculations to better understand these anomalous systems.[1] Models for resonant modes usually start with an anharmonic oscillator model such as that used by Kirby[7] to characterize the properties of KI:Ag^+. The numerous effects seen experimentally in KCl:Li^+ have been adequately explained by the Gomez-Bowen-Krumhansl (GBK) model.[8] GBK assumed a potential consisting of eight harmonic wells constructed from the one-dimensional harmonic-oscillator potential.

In 1969, Quigley and Das[9] showed analytically how KCl:Li^+ would give rise to off-center behavior while KBr:Li^+ would produce on-center behavior. The key to the problem is the sensitivity of the minimum-energy configurations to the Born-Mayer parameters. The local potential at the impurity site results from a competition between the repulsive Born-Mayer potential and the attractive polarization terms. The repulsive terms which tend to keep the impurity on center fall off more rapidly with distance than the polarization terms. Therefore expansion of the lattice should favor off-center behavior. The expansion from KCl to KBr does not insure that the Li^+ ion will be off center in KBr, however, because the Li-Br repulsive potential is much stronger than the Li-Cl repulsive potential. The net result at low temperature is that the KBr:Li^+ is on-center. (Earlier calculations by Wilson *et al.*[10] did not predict the correct low-temperature behavior for KBr:Li^+; this discrepancy is probably due to their use of

room-temperature lattice parameters.)

Further experiments on KBr:Li^+ have shed much light on the nature of the potential for this impurity-host combination. The large far-infrared isotope effect coupled with the absence of a large electric field shift have led to use of a potential of the harmonic-oscillator form with an incipient barrier in the center.[1] The small barrier produces a large isotope effect without producing a large dipole moment for the Li ion. This barrier is a marked feature of the KCl:Li^+ system and has led us to use hydrostatic pressure to look for a bridge between the two kinds of defect motion.

Section II contains a description of the cryostat, pressure cell, and pressure-generating techniques. The data collected on the resonant modes in NaCl:Cu^+, KBr:Li^+, KI:Ag^+, and CsI:Tl^+ and the tunneling transition in KCl:Li^+ are presented in Sec. III. Isotope effect measurements on both KCl:Li^+ and KBr:Li^+ show that both lattice defect systems become more harmonic with increasing lattice strain. These data are analyzed in Sec. IV. The resonant modes shift as expected for an anharmonic oscillator. For the tunneling transitions the GBK model cannot be used for handling states near or above the potential barrier since it relies on a perturbation calculation employing the tunneling matrix element between adjacent wells. We have used the same harmonic-oscillator model but calculated the energy levels directly. To our surprise this potential fails to adequately describe the pressure dependence of the five observed absorption lines in KCl:Li^+ even at relatively low strain. As the potential is adjusted to the frequency of the lowest-frequency tunneling mode the potential approaches that of a harmonic oscillator too rapidly with strain to explain the higher-frequency transitions which are observed. A more anharmonic square well with a square barrier is found to represent all the data more accurately. The results are summarized in Sec. V.

II. EXPERIMENTAL TECHNIQUES

The far-infrared absorption spectra were taken with a lamellar interferometer[11] interfaced to a PDP-11 computer.[12] The cryostat containing the high-pressure cell is shown in Fig. 1. The far-infrared radiation passes through the pressure cell to a ^{3}He-cooled bolometer detector.[13] Because the pressure cell produced a tenfold decrease in the far ir throughout this sensitive bolometer was required to obtain spectra down to 3 cm^{-1}.

The major components of the detector cryogenics are shown in Fig. 2. A self-contained ^{3}He charcoal adsorption pump[14] is used to keep the detector temperature between 0.30 and 0.31°K for up to 24 h.

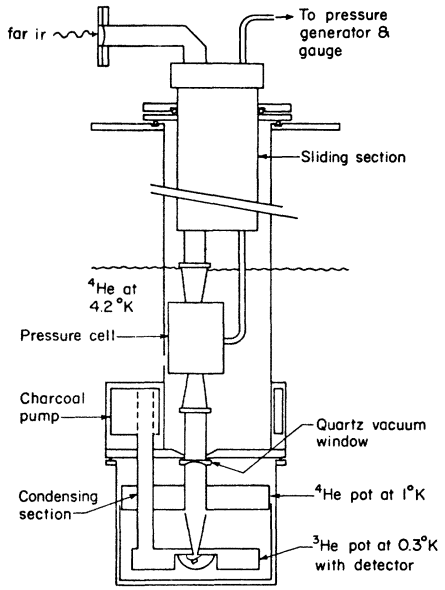

FIG. 1. Detector cryostat with pressure insert. The far-infrared radiation (far ir) passes down the light pipe through the pressure cell to the ^{3}He-cooled bolometer detector. The components are identified in the figure.

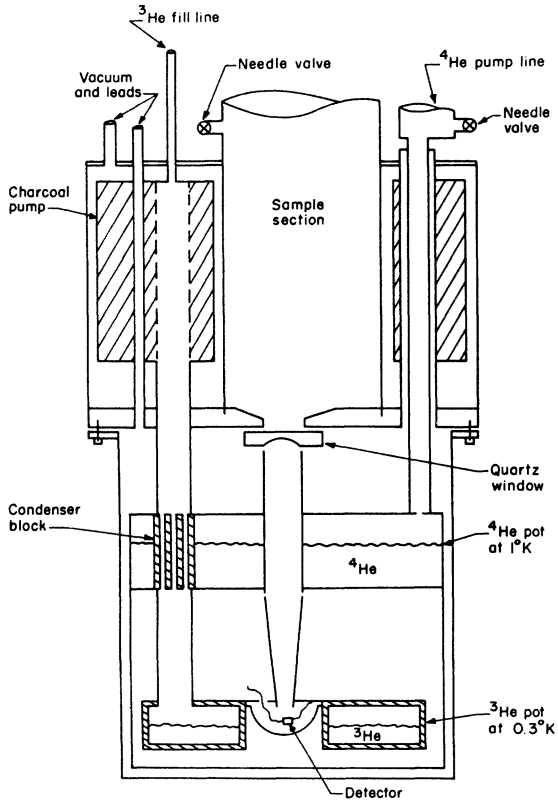

FIG. 2. Detailed schematic of detector and associated absorption pump assembly. A complete description is given in the text.

This charcoal pump, which is in cross section an eccentric annulus surrounding the sample section, is located in a vacuum can. The 400-cm^3 volume is filled with coconut charcoal from A.D. Little Co. This charcoal has a relatively large grain size, about 2 mm, so that the ^{3}He gas can circulate freely. The pump line from the ^{3}He pot is a $\frac{3}{8}$-in.-diam stainless-steel tube joined to a copper condenser block which is in contact with the 1°K-^{4}He pot. The ^{3}He fill line is a $\frac{1}{8}$-in. tube which extends from the charcoal pump to the cryostat top plate where a pressure gauge is in series with a high-pressure valve. At room temperature the three STP liters of ^{3}He gas in the chamber produce a pressure of 12 atm. The operation of this pump is straightforward and has been described earlier.[15]

The pressure apparatus was designed so the pressure cell could be raised out of the ^{4}He bath with the cryostat still sealed from the atmosphere. This step is necessary when changing pressure because helium solidifies at these low temperatures (for example, at 8 kbar ^{4}He freezes at about 50 K).

Figure 3 is a schematic representation of the pressure cell. The cell body is heat treated maraging steel, whereas the entrance and exit light cones and the mushroom plugs are constructed of heat treated beryllium copper. The seals are the Bridgeman unsupported area type after a design by Fitchen.[16] The presence of two dissimilar metals had no effect on the pressure integrity of the cell

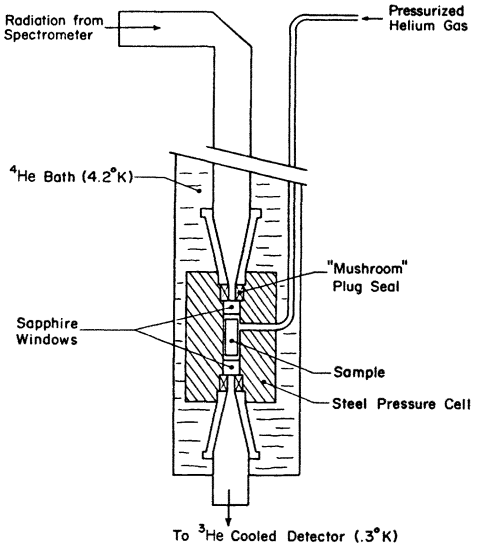

FIG. 3. Schematic representation of the far-infrared pressure cell. The radiation passes through a sapphire window the sample and another sapphire window. The sapphire forms a Poulter seal with a Bridgeman unsupported area-type mushroom plug. The pressure medium is ^{4}He gas.

during temperature cycling. The optical aperture of the cell is 0.125 in. and the bore is 0.260 in. The sapphire windows are transparent below 400 cm^{-1} for temperatures below 40°K.

To take data the cell is pressurized at room temperature to the maximum pressure (typically over 8 kbar). After cooling the cryostat to 77°K the cell is repressurized to make up for the temperature-induced pressure drop. Finally liquid helium is transferred. To change the pressure the cell is lifted out of the helium bath and warmed to the point where the solid helium melts. A small but measurable drop in the manganin gauge pressure occurs at this temperature. The pressure is then slowly changed to the next desired value by loosening one of the pressure fittings. The temperature at which solidification occurs again produces a rapid change in the pressure reading.

The final pressure in the pressure cell at 4.2°K is obtained by correcting the gauge reading at the melting temperature for the thermodynamic loss of pressure expected after the blockage of the capillary tubing feeding the pressure cell. The solid helium then cools at constant volume. The error in the gauge reading is estimated to be ±0.01 kbar. The error in the correction depends mainly on how well the approximation of cooling at constant volume works. If the block in the tubing slips then the calculated correction will be much larger than the real correction. Based upon many experiments we estimate the total errors to be +0.2, −0.05 kbar. The highest pressure obtainable at 4.2 K was 7.7 kbar and was limited by the pressurizing equipment rather than the strength of the cell, windows or other static parts.

All crystals were grown by the crystal growing facilities of the Materials Science Center at Cornell. The crystals were grown by the Kyropoulos technique with a boule size of approximately 1 in. diam by 4 in. The dopant concentrations are given in Table I. Samples were cleaved from the boule, mounted on a rod, and turned down on a lathe to

TABLE I. Sample record.

No.	Boule No.	Host	Dopant	Dopant concentration (molar % in melt)
1	7 102 241W	KBr	^{6}LiBr, ^{7}LiBr	0.01% each
2	7 206 204W	KBr	^{6}LiBr	0.5%
3	7 106 086W	KCl	^{6}LiCl	0.5%
4	7 108 272G	KCl	^{6}LiCl	0.05%
5	7 111 051W	KCl	^{6}LiCl, ^{7}LiCl	0.02% each
6	7 208 021W	KI	AgI	0.5%
7	7 302 214W	NaCl	CuCl	0.0015%
8	7 303 161W	CsI	TlI	0.01%

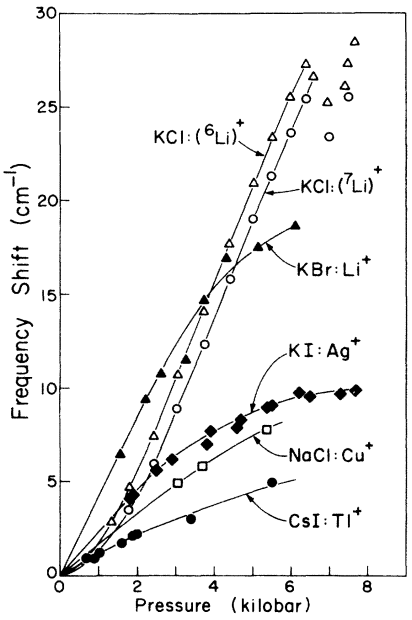

FIG. 4. Measured hydrostatic pressure shift of resonant and tunneling modes.

0.250 in. diam. The possibility of inducing strains by this method was checked by comparing the experimental results of unannealed and annealed specimens. The absorption lines appeared at the same frequencies for a given pressure in both unannealed and annealed samples and the line widths were similarly the same.

III. EXPERIMENTAL RESULTS

To obtain an accurate measure of the center frequency of an absorption line it is necessary to divide out the source spectrum of the interferometer. For our pressure measurements it has not been possible to measure both a pure and doped sample at the same time. The comparison spectrum, therefore, is always the zero pressure spectrum. When the measured frequency shifts are larger than the linewidth of the mode being investigated this technique works quite well. Only in the case of KCl:Li^+ did we experience a problem due to the additional excited-state transitions near 40 cm^{-1}. Most of this section will be concerned with the complex experimental results obtained for KCl:Li^+. Before turning to this problem we shall describe the relatively simple behavior of the pressure shift observed for resonant-mode systems.

A. Resonant modes

Figure 4 shows the experimental frequency shifts versus pressure for all of the low-frequency impurity modes which we have measured. In no case is a linear pressure shift observed. For the resonant mode systems KBr:Li^+, KI:Ag^+, NaCl:Cu^+, and CsI:Tl^+ the shift is linear at small pressure but is quite nonlinear above 2 kbar. The KCl:Li^+ tunneling transition, on the other hand, is linear at high pressures but not at small. Another feature of this data is that all the shifts are within an order of magnitude of each other. Finally no simple relation exists between the shift and the mode frequency at zero pressure (Table I, column 1). To put these data in a more fundamental form it is convenient to refer to the crystal strain rather than the pressure. The strain can be related to the pressure with an equation of the form

$$-\frac{dV}{V} = 3(S_{11}+2S_{12})P - 3\delta P^2 , \tag{1}$$

where the first pressure coefficient is the isothermal compressibility and second nonlinear term is typically 5% of the first term for pressures around 5 kbar. These coefficients are given for pure crystals in columns 3 and 4 of Table II. The first coefficient has been measured at 4.2 °K

TABLE II. Hydrostatic-stress coupling coefficients for infrared-active modes.

Defect system	Mode frequency (cm^{-1}) $P=0$ (Ref. 1)	Bulk $S_{11}+2S_{12}$ (4.2 °K) (10^{-3} $kbar^{-1}$) (Ref. 1)	Bulk δ(300 °K) (10^{-6} $kbar^{-2}$) (Ref. 17)	V_A [(unit strain)$^{-1}$]	A (cm^{-1}/unit strain)
NaCl:Cu^+	23.4	1.253	13	34	398
KCl:(^{6}Li)$^+$	1.15	1.691	20	...	...
KCl:(^{7}Li)$^+$	0.82				
KBr:(^{6}Li)$^+$	17.71	1.907	13	105	887
KBr:(^{7}Li)$^+$	16.07				
KI:Ag^+	16.35	2.618	20	39	319
CsI:Tl^+	14.1	2.313	37	23	162

while the second coefficient has been measured at 300°K. We have used both of these values to present our data in terms of lattice strain. The compliance constants have not been modified to account for a softening of the lattice in the neighborhood of the impurity.[18]

Although taking the frequency shifts shown in Fig. 4 and plotting the data versus lattice strain still gives nonlinear shifts in every case, we have found that a linear dependence on lattice strain exists for resonant modes when $[\omega^2(\Delta a/a) - \omega_0^2]/\omega_0^2$ is plotted versus lattice strain. If we assume that the resonant-mode frequency can be written

$$\omega^2(\Delta a/a) = k(\Delta a/a)/m\,, \tag{2}$$

where m does not depend on the lattice strain, then

$$\Delta k/k_0 = [\omega^2(\Delta a/a) - \omega_0^2]/\omega_0^2 = 3V_A(\Delta a/a)\,. \tag{3}$$

The observed linear dependence of the resonant-mode force constant on lattice strain is shown in Fig. 5 for KBr:Li^+, NaCl:Cu^+, and CsI:Tl^+. The coefficient V_A is given in Table II, column 5. For KI:Ag^+ even this dependence is nonlinear as shown in Fig. 6. Both a linear and quadratic dependence are required to fit the measured force constant change with

$$(\Delta k/k_0)(\text{KI:Ag}^+) = 117(\Delta a/a) - 14.6(\Delta a/a)^2\,. \tag{4}$$

The largest resonant mode shifts have been observed for KBr:Li^+. Two pressure runs were made on a single sample (No. 1 in Table I) which contained roughly equal amounts of ^{6}Li and ^{7}Li dopant. The centroid of the double line was taken to give the data in Fig. 4. The plot of the absorption coefficient versus frequency for five strains

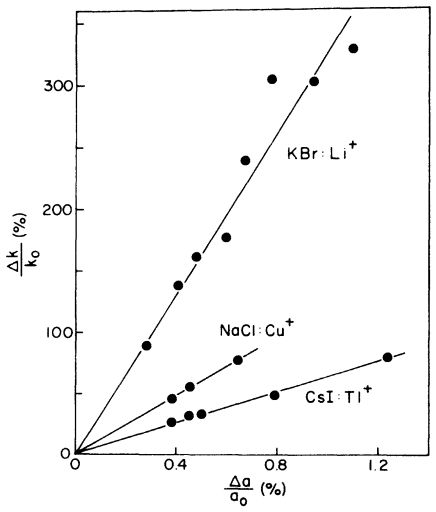

FIG. 5. Linear dependence of the resonant mode force constant with hydrostatic strain.

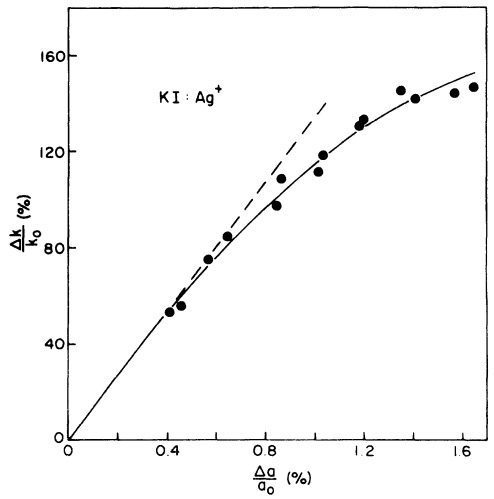

FIG. 6. Nonlinear dependence of the resonant mode force constant in KI:Ag^+ with hydrostatic strain.

is shown in Fig. 7. In addition to the centroid shifting rapidly with increasing strain the frequency separation between the two peaks decreases and the line width increases. The integrated area under the absorption curve is constant as a function of strain within experimental error (±20%). We can place an upper limit of 3% on the isotope shift at the highest strain while the isotope shift at zero pressure is 10%. Our last experiment on KBr:Li^+ was with a high-concentration sample (No. 2 in Table I) at zero pressure. In addition to the strong line at 17.7 cm^{-1} we also observed two weak lines at 43.7 and 53.3 cm^{-1} in reasonable agreement with earlier work.[6]

B. KCl:Li^+

The plot of the absorption coefficient versus frequency for sample 3 in Table I at 0.275% strain

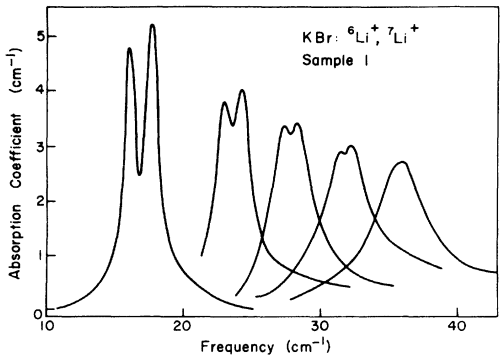

FIG. 7. KBr:Li^+ absorption spectra at five strains. The five strains are from left to right (0, 0.291, 0.482, 0.674, and 1.07)%. The isotope effect disappears with increasing strain. Sample No. 1 in Table I.

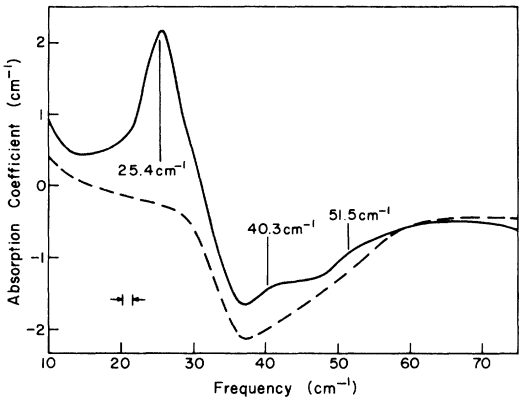

FIG. 8. KCl:$(^6Li)^+$ absorption spectrum for a high-concentration sample (No. 3) at 0.275% strain. The solid curve represents the absorption relative to the same sample at zero strain. The dashed curve represents the zero strain absorption relative to a pure sample and must be subtracted away in order to observe the three peaks indicated.

compared to zero strain is shown in Fig. 8. To extract the frequencies of the absorption lines associated with this spectrum the zero strain absorption must be subtracted. The dashed curve in this figure is a construction of the zero strain absorption coefficient made by hand from many curves at various strains with the zero pressure data of Kirby *et al.*[19] as a guide. The subtraction of this dashed curve from the experimental spectrum yields three readily observable absorption lines at the frequencies indicated. Repeated use of this technique on a number of samples at a variety of pressures has allowed us to identify and study the five absorption lines shown in Fig. 9.

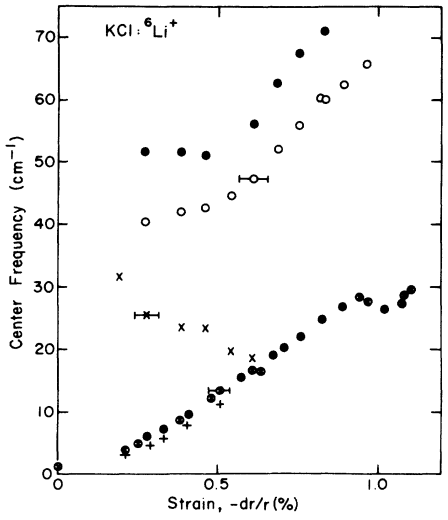

FIG. 9. Strain dependence of KCl:$(^6Li)^+$ absorption frequencies. The three high-frequency lines are not resolved at zero strain.

The three highest-frequency transitions in Fig. 9 which are not resolved at zero strain are weak and have been measured in the high-concentration sample (No. 3 in Table I). The two highest-frequency lines were measured versus strain until their frequencies increased beyond the range of the interferometer. These lines broadened considerably with increasing frequency. Because of base line problems together with the large width of these relatively weak lines it is not possible to assign a realistic halfwidth to each of these lines but the widths were at least 15 cm^{-1} at the largest strains. The lowest-frequency line of this triplet decreases in frequency and strength with increasing strain.

The two lowest-frequency lines in Fig. 9 correspond to transitions within the lowest tunneling multiplet. The lowest-frequency line is not observed in the high-concentration samples because the very strong main tunneling transition is broadened by the large concentration. Data for both of these lines comes from samples 4 and 5 in Table I. A typical absorption curve for unsmoothed data at 0.213% strain is shown in Fig. 10. The higher-frequency transition is from the ground state to the first excited state and the lower frequency corresponds to a transition from the first excited state to the second excited state. This identification was confirmed by varying the sample temperature at high pressure. The dashed curve in both parts of Fig. 11 represents the absorption coefficient at 0.406% strain at 4.3 °K. In Fig. 11(a), the effects of raising the temperature are shown. The ground-state transition decreases in strength sharply while the lower-frequency line originating from the excited state increases in strength. Both effects are consistent with population changes within

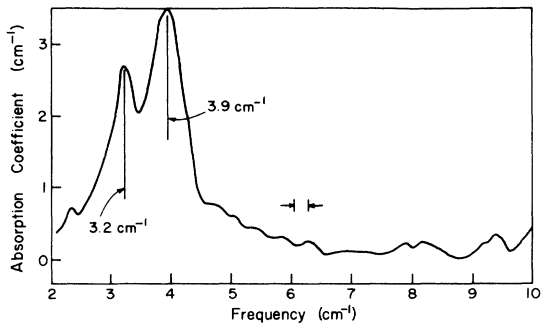

FIG. 10. KCl:$(^6Li)^+$ absorption spectrum (sample No. 4) at 0.213% strain showing unsmoothed data. The two absorption peaks indicated are due to transitions within the tunneling multiplet. The higher frequency is for a transition from the ground state to the first excited state and the lower frequency corresponds to a transition from the first excited state to the second excited state.

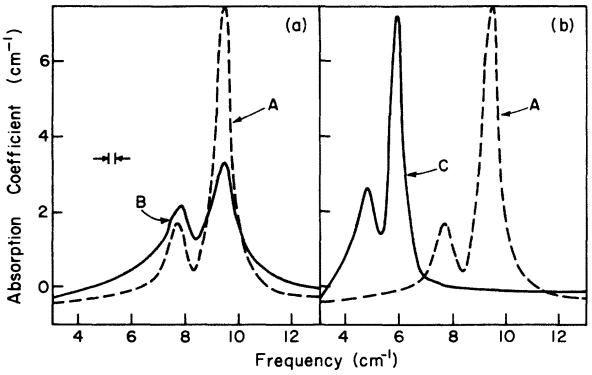

FIG. 11. (a) Temperature dependence of low-frequency absorption in KCl:$(^6Li)^+$. (b) Pressure dependence. Curve *A* was taken at 0.406% strain and 4.3 K. Curve *B* was taken at 0.406% strain and 15 K. Curve *C* was taken at 0.297% strain and 4.3 K. The two absorption lines are due to transitions within the tunneling multiplet as described in Fig. 10. Sample was No. 4.

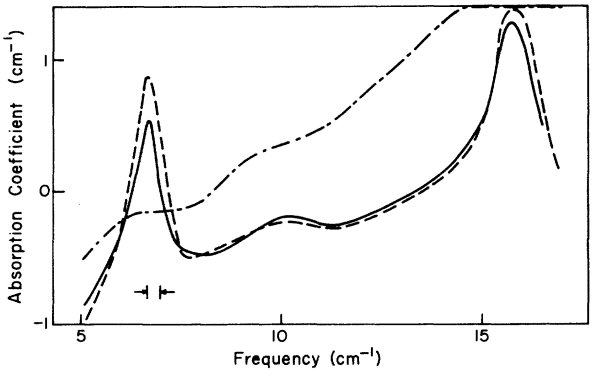

FIG. 12. KCl:$(^6Li)^+$ absorption spectrum (sample No. 3) at 0.837% strain for frequencies below the tunneling mode. The tunneling mode is at 21.2 cm^{-1}. These lines are probably pair modes. The dashed curve was taken at 2 K, the solid curve at 4.3 K, and the third curve at 15 K.

the multiplet. Figure 11(b) shows the effects of lowering the pressure. The drop in frequency of the absorption lines indicates that the energy level splittings become smaller with decreasing strain. Again the ground-state population should be reduced and the excited-state population increased leading to qualitatively the same effect as for the temperature rise. This is indeed what is observed as the tunneling line is reduced slightly in strength while the lower-frequency line picks up strength. This result also indicates that the lower-frequency transition will disappear with application of sufficient strain and indeed this is the case as shown in Fig. 8.

An additional feature seen in Fig. 9 is the anomaly in the strain dependence of the main tunneling transition for large strain. Data points giving this dip come from two separate experiments. An examination of this curve indicates that only one point, the point at 0.63% strain, seems out of line from a smooth curve; however the deviation is much less than the magnitude of the dip. The size of the errors leads us to conclude that this anomalous dip may be real.

Several weak absorption lines are observed at frequencies below the tunneling absorption in the high-concentration sample. Two such lines are shown for 0.837% strain at three temperatures in Fig. 12. The lines at 6.7 and 15.8 cm^{-1} are well below the tunneling line at 21.2 cm^{-1}. The loss of absorption strength with increasing temperature is a clear indication that these lines involve a transition from a ground state. In the next section, it will be shown that these lines are totally inconsistent with the accepted model of KCl:Li^+ while the rest of the data confirms the picture. It is quite likely therefore that these lines are due not to single Li^+ impurities but either to some unwanted impurity or impurities or more likely to pair modes, that is, vibrational modes involving two nearby Li^+ ions.

The isotope shift is resolvable for the strongest tunneling mode transition even at the largest strains. Figure 13 shows a typical absorption curve for the two isotopes in a single sample at 0.893% strain. The strain dependence of the isotope effect is summarized in Fig. 14. Here $\Delta\omega$ equals $\omega(^6Li)-\omega(^7Li)$ and is divided by the average of the two frequencies.

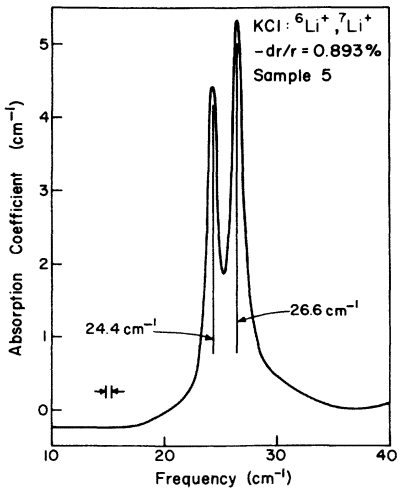

FIG. 13. Absorption spectrum at 0.893% strain for a sample containing both lithium isotopes. The transition responsible for the lines is from the ground state to the first excited state.

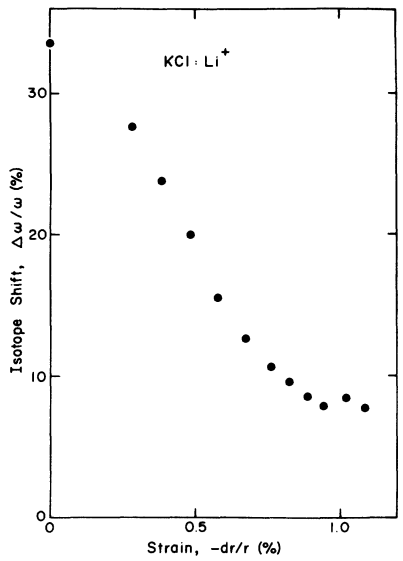

FIG. 14. Strain dependence of KCl:Li^+ isotope effect for the transition between the ground state and the first excited state of the system. $\Delta\omega$ is ω for $(^6Li)^+$ minus ω for $(^7Li)^+$ and the ω in $\Delta\omega/\omega$ is the average of the two.

IV. DISCUSSION OF THE EXPERIMENTAL RESULTS

A. Resonant modes

A simple interpretation of the linear spring constant variation with lattice strain can be obtained from the anharmonic oscillator model.[7] If third-order anharmonic coupling is assumed to be important for all resonant modes then the hydrostatic pressure shift of the T_{1u} resonant mode is of the form

$$H' = -\tfrac{1}{2}k_0 r^2 V_A \epsilon_{A_{1g}} , \tag{5}$$

where V_A is the coupling constant to lattice strains of A_{1g} symmetry and $\epsilon_{A_{1g}} = \Delta V/V$ is the hydrostatic strain. The Hamiltonian of the resonant mode can be written

$$H = (P^2/2m^*) + \tfrac{1}{2}k_0(1 - V_A\epsilon_{A_{1g}})r^2 , \tag{6}$$

where k_0 is the force constant of the unperturbed oscillator. The effective force constant in the presence of hydrostatic strain is

$$k = k_0(1 - V_A\epsilon_{A_{1g}})$$

so

$$\Delta k/k_0 = -V_A\epsilon_{A_{1g}} = (\omega^2 - \omega_0^2)/\omega_0^2 . \tag{7}$$

The hydrostatic coupling coefficient A is defined by

$$\Delta\omega \equiv -A\Delta V/V . \tag{8}$$

At zero strain the anharmonic coupling coefficient V_A is related to the hydrostatic coupling coefficient A by

$$\tfrac{1}{2}V_A = A/\omega_0 . \tag{9}$$

The coupling coefficients are given in Table II.

For three resonant modes systems the force constants do vary linearly with strain as illustrated in Fig. 5. KI:Ag^+ is anomalous in this respect, for in addition to the linear contribution the resonant mode shift contains a large quadratic dependence on strain. From the experimental data in Fig. 6 it is projected that the frequency shift for KI:Ag^+ will reach a maximum at about 6% lattice strain and then decrease for larger lattice strains. If one assumes that the coupling to dynamic strains is the same as the static strains, then for most of the resonant mode systems which we have studied linear coupling is sufficient. For KI:Ag^+ one should include quadratic coupling as well.

B. KCl:Li^+

The spectroscopic information which has been made available by the hydrostatic pressure measurements enables us to probe the detailed shape of the multiwell potential associated with ionic tunneling. To determine how different characteristic parameters affect the experimental data we first enumerate the general properties of a double well potential. Let us consider two wells at $\pm\infty$. The energy-level scheme of this potential will consist of a set of doubly degenerate levels. As the wells are brought in from infinity the barrier between them becomes finite. As the tunneling probability increases the degeneracy will be lifted and the energy-level scheme will consist of pairs of closely spaced levels for energies less than the barrier. Eventually as the well separation approaches zero the level splitting will become large and the final-level scheme is a set of levels with the same energy as the two wells at infinity except the levels are nondegenerate. We are mainly interested in the potential associated with the intermediate region which we shall call $V(x)$ with potential minima at $\pm a$. To model KCl:Li^+ we must extend our potential to three dimensions. The simplest three-dimensional potential with the correct symmetry is

$$V(x, y, z) = V(x) + V(y) + V(z) . \tag{10}$$

If $V(x)$ has two minima at $\pm a$ then $V(x, y, z)$ has eight minima at $(\pm a, \pm a, \pm a)$ (along the [111] directions). For a potential of this form the Schrödinger equation is separable in the three coordinates and the level energies E_n are the sum of the energies for the three separate one-dimensional potentials. If we use a prime to denote the energy levels of the one-dimensional potential then the lowest state

has an energy $E_0 = 3E_0'$, and is nondegenerate. The second level's energy is $E_1 = 2E_0' + E_1'$. Since there are three ways to construct this sum the level is triply degenerate. The entire set of energy levels which can be constructed by similar arguments is shown in Fig. 15. We have labeled these levels with the appropriate irreducible representations of the O_h symmetry group. The vertical arrows refer to allowed electric dipole transitions from any of the states in the lowest multiplet. All of these 13 transitions will occur for KCl:Li^+ at 4.2 K since the relative Boltzmann populations of these levels for ^{6}Li impurities are A_{1g}—21%, T_{1u}—43%, T_{2g}—29%, and A_{2u}—7%. As the pressure changes the splittings between levels some of the transitions from the excited states will naturally disappear. Since hydrostatic pressure does not change the symmetry of the potential Fig. 15 is representative of the energy level scheme for all pressures.

The 13 transitions do not all occur at different frequencies. The following equalities hold true for all potentials of the form $V(x,y,z) = V(x) + V(y) + V(z)$:

$$\omega_1 = \omega_2 = \omega_3, \quad \omega_4 = \omega_7, \quad \omega_6 = \omega_9 = \omega_{12}, \quad \omega_5 = \omega_8 = \omega_{11}, \quad \omega_{10} = \omega_{13}. \tag{11}$$

The remaining frequencies are not uniquely determined as evidenced by the following relation:

$$\omega_4 = \omega_6 + 2\omega_1. \tag{12}$$

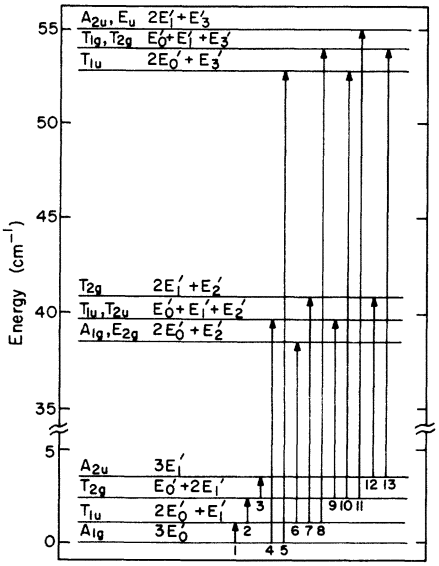

FIG. 15. Energy-level diagram of an eightfold potential well formed from a double-well potential $V(x)$ by the summation $V(x) + V(y) + V(z)$. The levels correspond approximately to those of KCl:$(^6Li)^+$.

A further point concerning the geometrical form of the potential $V(x,y,z)$ is worth noting. The relative magnitudes of the potential maxima are also invariant with respect to the particular choice of potential. If V_0 is the barrier between adjacent wells then the central barrier of the potential at the origin is $3V_0$ while the barrier between two wells across a face of the cube formed by the eight wells is $2V_0$.

Keeping thse various points in mind, we now proceed to compare the experiments with particular models.

1. *Double-hamonic-oscillator model*

In order to maintain continuity with previous theoretical approaches we shall investigate the double harmonic oscillator (DHO), the potential of the GBK model. As we are only interested in the energy levels, the GBK perturbation approach will be abandoned in favor of a direct calculation of these levels by integrating the Schrödinger equation with trial values of the energy.

At zero strain it is possible to fit the known data on the energy level scheme of KCl:Li^+ with the DHO potential. It turns out, however, that it is possible to do as well with almost any double well potential by varying its parameters in an appropriate manner. The presence of a large barrier is much more significant than the details of the actual potential.

In the DHO model when the off-center distance goes to zero, the system becomes harmonic and $\omega_6 \to \omega_1$. At this point the energy levels are almost equally spaced. Since the harmonic oscillator selection rule is $\Delta N = 1$ only one absorption should be seen. If we allow some anharmonicity the $\Delta N = 3$ transition should be weakly allowed.

Transition ω_6 represented by the X's in Fig. 9 becomes the same as ω_1 (the strong tunneling line) at 0.65% strain. The spectrum indicates that the Li^+ ion is on center at this strain; however, the two lines at higher frequency have not weakened as expected for the DHO model. As the potential is adjusted to the frequency of the lowest-frequency tunneling mode the potential approaches that of a harmonic oscillator too rapidly with strain to explain the high-frequency transitions which are observed. It appears that the system is more anharmonic than predicted by the DHO model.

2. *Square well with a square barrier*

Since we have just shown that the individual potential minima are not harmonic there seems little reason to continue with the DHO model. To study how pressure affects the potential barrier an anharmonic potential is required. The square

well with square barrier is especially attractive for this purpose as the barrier height and width are represented individually by two separate parameters, for the DHO the amplitude of the barrier also influences its width while the off-center distance similarly affects the amplitude.

For the square well with square barrier transcendental equations were developed for the energy and were solved by using trial values for the energy. Three parameters are available: the potential width, the barrier width, and the barrier height. The experimental data consists of five absorption lines plus the isotope effect. At four strains the parameters were chosen so as to best fit the data. The results of these calculations are given in Table III for the potentials pictured in Fig. 16. All data and calculations shown are for $^6Li^+$ impurities.

The zero-pressure data has been gathered from a number of sources. The absorption band at 40 cm^{-1} is made up of many separate transitions the centroid of which exhibits a negative isotope effect, that is the heavier $^7Li^+$ impurity absorbs at higher frequencies than does the lighter $^6Li^+$. The band is quite asymmetric and is weighted more strongly to the low-frequency side.[1] The peak is at 37 cm^{-1} which we assign to the single transition frequency ω_6 in Table III. Various techniques have shown the zero-pressure splitting of the tunneling levels to be around 1 cm^{-1}. Of special interest are the EPR measurements of Herendeen and Silsbee[21] which established the ground-state splitting of $(^6Li)^+$ to be 1.15 cm^{-1} and the phonon spectroscopy work of Hetzler and Walton[22] which showed that the first-excited-state transition was about 72% of this value. The isotope shift of this tunneling transition is of the normal sign but with the unusually large value of 33.5%.

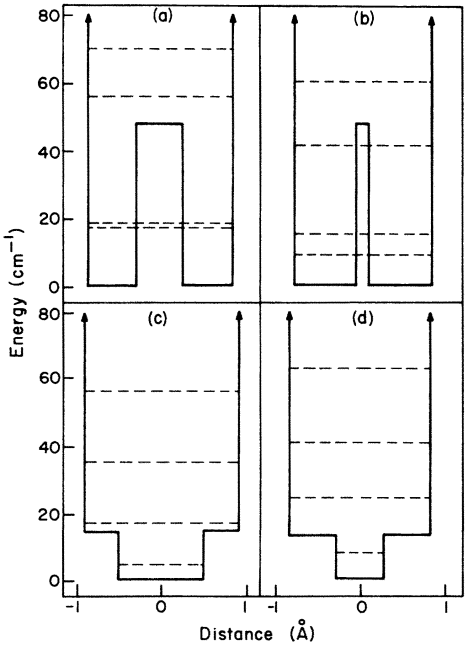

FIG. 16. Potentials which best fit data for (a) 0% strain, (b) 30% strain, (c) 0.5% strain, and (d) 0.6% strain. The dashed lines are the four lowest energy levels in one dimension.

Figure 16(a) shows the potential which best fits the data for zero strain. Our simple potential requires that $\omega_1 = \omega_2$ which does not agree with the experimental results in Table II. This discrepancy could be eliminated by choosing a potential with components $V(x) \neq V(y) = V(z)$. Because we are mainly interested in the pressure dependence of the barrier we shall not incorporate this refinement into our model. Additional predicted transitions occur above 37 cm^{-1} in agreement with the experimental transitions in the broad 40-cm^{-1} band. The calculated isotope effect for the ground-state transition in Fig. 16(a) is 48%, which is in fair agreement with the experimental value. The negative isotope effect of the excited-state transition cannot be obtained from static tunneling potentials and thus we cannot use this experimental information in the present model. A possible ex-

TABLE III. Absorption frequencies for KCl:$(^6Li)^+$ square-well model and experimental data.

Strain (%)	Label	Frequency (Theor.) (cm^{-1})	Frequency (Expt.) (cm^{-1})
0	ω_2	1.16	0.83
	ω_1	1.16	1.15
	ω_6	37.4	37.0
	ω_4	39.7	
	ω_5	52.8	
	ω_{10}	50.5	
0.3	ω_2	5.9	5.0
	ω_1	5.9	5.9
	ω_6	26.3	26.3
	ω_4	38.1	40.4
	ω_5	51.4	51.4
	ω_{10}	39.6	not observed
0.5	ω_2	12.7	10.4
	ω_1	12.7	12.7
	ω_6	18.1	20.6
	ω_4	43.5	43.5
	ω_5	51.9	51.9
	ω_{10}	26.5	not observed
0.6	ω_2	16.3	14.0
	ω_1	16.3	16.3
	ω_6	16.6	18.9
	ω_4	49.2	47.1
	ω_5	55.6	55.4
	ω_{10}	23.0	not observed

planation of this negative isotope effect has been offered by Benedek.[20]

For a strain of 0.3% Fig. 16(b) shows the best fit for the potential. The experimental and calculated frequencies are given in Table III. The two lowest tunneling splittings are still unequal but the experimental ω_2 is now 84% of ω_1. This result indicates that the wells have become more spherical. All the other measured lines can be explained by the potential of Fig. 16(b). The data even satisfy Eq. (12). The isotope effect is also in agreement for this strain. The data shows a 27% effect for the tunneling splittings and the predicted effect is 25%. The significant differences between the potentials for zero strain and 0.3% strain is seen to be a strong narrowing of the potential barrier. The total well width of the double well is also slightly reduced by 4.6%. The barrier height does not change although this would probably not be true for a realistic potential.

When the strain reaches 0.5% the nature of the potential has changed considerably as shown in Fig. 16(c). The results in Table III indicate that this potential adequately describes the observed transition frequencies. Experimentally the ratio of ω_2/ω_1 appears to remain constant at all strains. Although a barrier is no longer necessary to fit the energy level scheme there still could be an incipient barrier present whose height is less than the ground-state energy. It would be possible to fit the energy levels with such a barrier if additional parameters were introduced to vary the shape of the sides of the potential well. Indeed the isotope shift for the potential of Fig. 16(c) is 11.5% while the observed shift of 19% is indicative of the presence of an incipient barrier.

For a strain of 0.6% we again find $\omega_2 \neq \omega_1$. The experimental value of ω_2 for this strain was obtained by extrapolation from lower strain data. This transition originates from the first excited state of the system and as expected has disappeared due to lack of thermal population of this state as the splittings become large. The situation regarding the possible presence of a barrier is the same as for 0.5% strain. The predicted isotope effect for the potential of Fig. 16(d) is 9.1% while the observed value is 14.2%. It seems likely that an incipient barrier still exists.

For the lower strains, we were able to fit exactly three of the four remaining observed absorption lines while coming close to the frequency of the fourth. At 0.6% this is no longer possible. Without the aid of additional parameters we are able to fit exactly only one frequency although the others are not far from the observed values. The model begins to break down and the agreement becomes worse at higher strains where only three transitions are observed. With the barrier suppressed the details of the potential are, no doubt, important.

TABLE IV. KCl:(^{6}Li)$^+$ vs KBr:(^{6}Li)$^+$ comparison.

	KCl:(^{6}Li)$^+$	KBr:(^{6}Li)$^+$
Strain	0.65%	0.0%
ω_1 frequency	17.7 cm^{-1}	17.7 cm^{-1}
ω_4 frequency	49.0 cm^{-1}	43.7 cm^{-1}
ω_5 frequency	58.5 cm^{-1}	53.5 cm^{-1}
Isotope effect	13.3%	9.7%

While measuring the absorption spectra of KCl:Li$^+$ at strains greater than 0.6, we were struck by the remarkable similarity of this spectra to that of KBr:Li$^+$ at zero strain. In each case three transitions were observed and the isotope effects were similar. Table IV details this comparison. The isotope effect for both systems indicates that the impurity ion is in an intermediate configuration between the off-center and on-center limit. A great many experiments on KBr:Li$^+$ at zero pressure have defined the appropriate Li$^+$ potential for this system.[22] Our experimental results indicate that this potential is the appropriate one for KCl:Li$^+$ at 0.65% strain as well.

V. SUMMARY

The hydrostatic pressure dependence of the far-infrared absorption spectra of resonant modes and tunneling states has been measured at low temperatures. The effect of pressure on the impurity isotope effect was studied in KCl:Li$^+$ and KBr:Li$^+$. Pressures as high as 7.7 kbar were generated for this purpose corresponding to strains as large as 1.1%.

Most resonant mode shifts were found to vary linearly when the force constant change is plotted versus strain. This dependence is a natural consequence of the cubic interaction between the T_{1u} mode and, even parity modes. KI:Ag$^+$ was anomalous in that both a linear and quadratic strain dependence was required to account for the experimental force constant change.

The multiple absorption lines in KCl:Li$^+$ underwent large frequency shifts with strain. With increasing strain the zero-pressure excited-state absorption centered around 40 cm^{-1} was resolved into three absorption lines; one of these lines decreased in strength with increasing strain and disappeared at 0.6% strain. Transitions between the low-lying tunneling levels were shifted into the far infrared where an unequal splitting of the tunneling levels were observed, in agreement with the experiments of Hetzler and Walton.[23] An anomalous

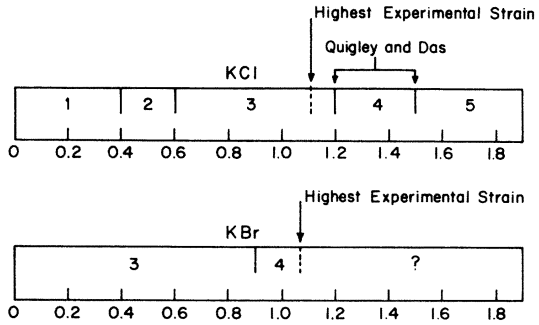

FIG. 17. Potential classification vs strain for KCl:Li^+ and KBr:Li^+ systems. The different regions are specified by numbers as follows: (1) off-center region, (2) barrier transitional region, (3) anharmonic region, (4) normal region, and (5) harmonic region.

dip in the frequency versus strain curve of the tunneling mode absorption was seen at the highest strains and remains without explanation. The disappearance of two of the lines with increasing strain is consistent with the associated decrease in Boltzmann population of the higher tunneling levels due to the pressure induced splittings.

The DHO potential used in the GBK model does not describe the many phenomena observed at intermediate strains. Instead we find that a square-well potential with a square barrier explains the pressure behavior of the multiple absorption lines in terms of a decrease in width of the potential barriers of the off-center system. Our simple model begins to break down, not unexpectedly, at about the same strain at which the data would indicate that Li^+ ion has gone "on center," a strain of 0.5%.

Hydrostatic pressure appears to be an important parameter by which one can transform the local potential in KCl:Li^+ into that found in KBr:Li^+. The strain dependence of this transformation is summarized in Fig. 17. The potential moves through several regimes in which the potential is (i) off center, (ii) in a barrier transitional region, where the ground state is above the barrier but the barrier still dominates the system, (iii) anharmonic, where local anharmonic effects in the potential dominate any barrier effects, (iv) normal, where anharmonic affects are weak but observable and (v) harmonic. The estimates of Quigley and Das[9] for strain at which the transitions to regions 4 and 5 occur for KCl:Li^+ are indicated in the figure.

Unfortunately the experimental results which we have obtained do not have the intrinsic high resolution quality characteristic of spectroscopic measurements because of the complications associated with low-temperature high-pressure measurements. More precise and complete measurements would be possible with the realization of a high-pressure optical cell with continuously tunable pressure at low temperatures. We have found that a wedding of far-infrared and high-pressure low-temperature techniques produces detailed information on the lattice constant dependence of the spectra associated with low-lying impurity modes. Finally, we have demonstrated that the wealth of spectral information potentially available can be used to identify precisely the particular energy configuration of the impurity ion.

---

*Work supported by the Energy Research and Development Administration under Contract No. E(11-1) 3151, Technical Report No. C00-3151-69. Additional support was received from the NSF under Grant No. DMR 72-003029 through the Cornell Materials Science Center, Report No. 2674.

†Present address: DuPont Experimental Station-Photo Products Dept., Wilmington, Del. 19899.

‡Present address: Hughes Research Lab., Malabu, Calif. 90265.

[1]A. S. Barker Jr. and A. J. Sievers, Rev. Mod. Phys. 47, 1–179 (1975).

[2]I. G. Nolt and A. J. Sievers, Phys. Rev. 174, 1004 (1968).

[3]B. P. Clayman, I. G. Nolt, and A. J. Sievers, Phys. Rev. Lett. 19, 111 (1967).

[4]H. S. Sack and M. C. Moriarty, Solid State Commun. 3, 93 (1965).

[5]G. Lombardo and R. O. Pohl, Phys. Rev. Lett. 15, 291 (1965).

[6]A. J. Sievers and S. Takeno, Phys. Rev. 140, A1030 (1965).

[7]R. D. Kirby, Phys. Rev. B 4, 3557 (1971).

[8]M. Gomez, S. P. Bowen, and J. A. Krumhansl, Phys. Rev. 153, 1009 (1967).

[9]R. J. Quigley and J. P. Das, Phys. Rev. 177, 1340 (1969).

[10]W. D. Wilson, R. D. Hatcher, G. I. Dienes, and R. Smoluchowski, Phys. Rev. 161, 888 (1967).

[11]I. G. Nolt, R. D. Kirby, C. D. Lytle, and A. J. Sievers, Appl. Opt. 8, 309 (1969).

[12]A. M. Kahan, Infrared Phys. 13, 25 (1973).

[13]H. D. Drew and A. J. Sievers, Appl. Opt. 8, 2067 (1969).

[14]D. Walton, T. Timusk, and A. J. Sievers, Rev. Sci. Instrum. 42, 1265 (1971).

[15]D. B. Tanner, Phys. Rev. B 8, 5045 (1973).

[16]D. B. Fitchen, Rev. Sci. Instrum. 34, 673 (1963).

[17]*American Institute of Physics Handbook*, 3rd ed. (McGraw-Hill, New York, 1972), pp. 4–38.

[18]G. Benedek and G. F. Nardelli, Phys. Rev. 167, 837 (1968).

[19]R. D. Kirby, A. E. Hughes, and A. J. Sievers, Phys. Rev. B 2, 481 (1970).

[20]G. Benedek, Phys. Status Solidi 43, 509 (1971).

[21]R. A. Herendeen and R. H. Silsbee, Phys. Rev. 188, 645 (1969).

[22]F. Bridges [see CRC Crit. Rev. Solid State Sci. 5, 1 (1975); Bull. Am. Phys. Soc. 21, 265 (1976)] has recently claimed that KBr:Li^+ is an off-center system. We have observed weak (strength $\leq 1/100$ of resonant mode transition) absorption lines below 5 cm^{-1} in the Bridges KBr:Li^+ crystals but have not observed these transitions in Cornell grown crystals. The source of these extra absorptions has not yet been identified but we speculate that they are associated with Li pairs or Li complex centers such as we have observed in KCl:Li^+ (see Fig. 12).

[23]M. C. Hetzler and D. Walton, Phys. Rev. B 8, 4812 (1973).